A

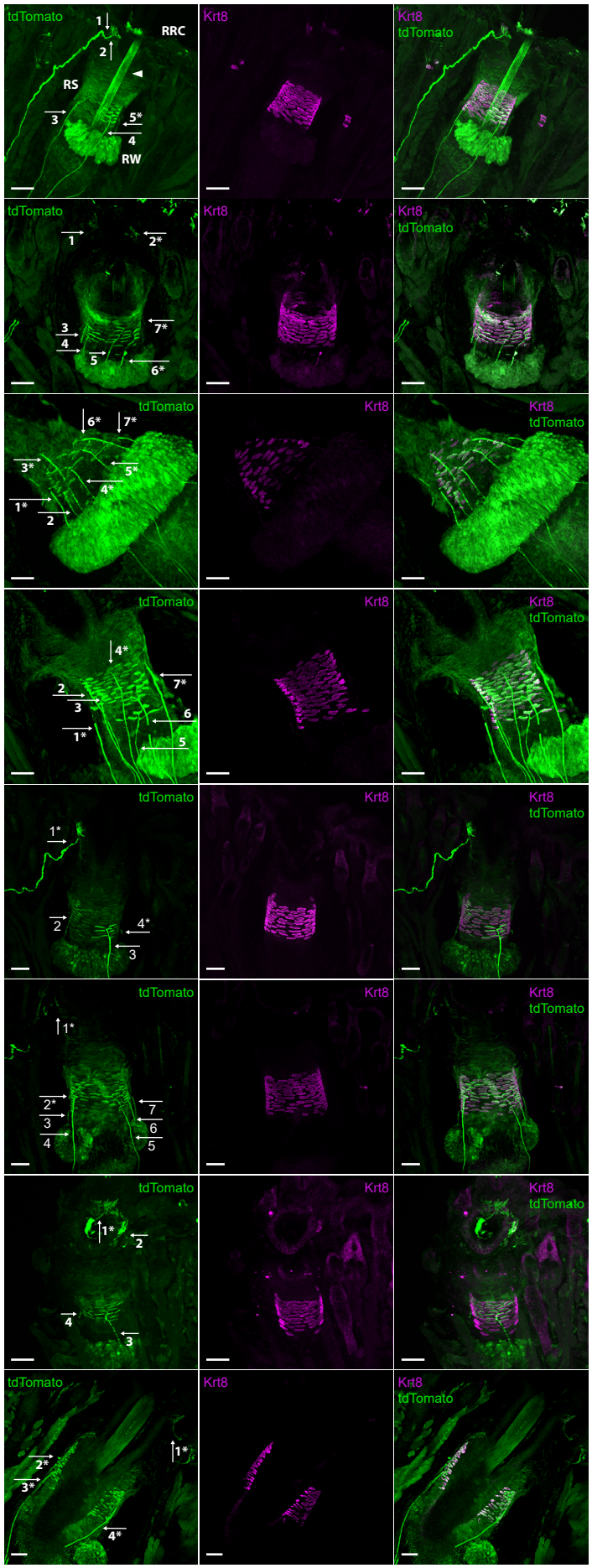

B

	Count	%
Merkel	1,045	99.2
Longitudinal lanceolate	2	.2
Club-like	6	.6
Total	1,053	

C

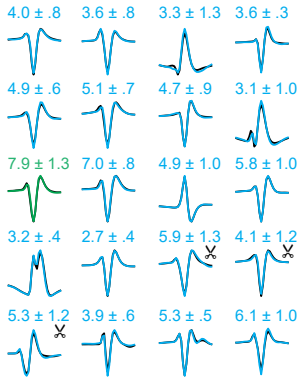

D

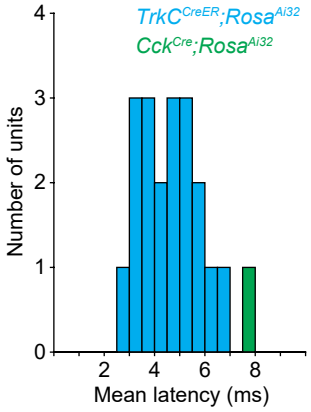

Figure S1

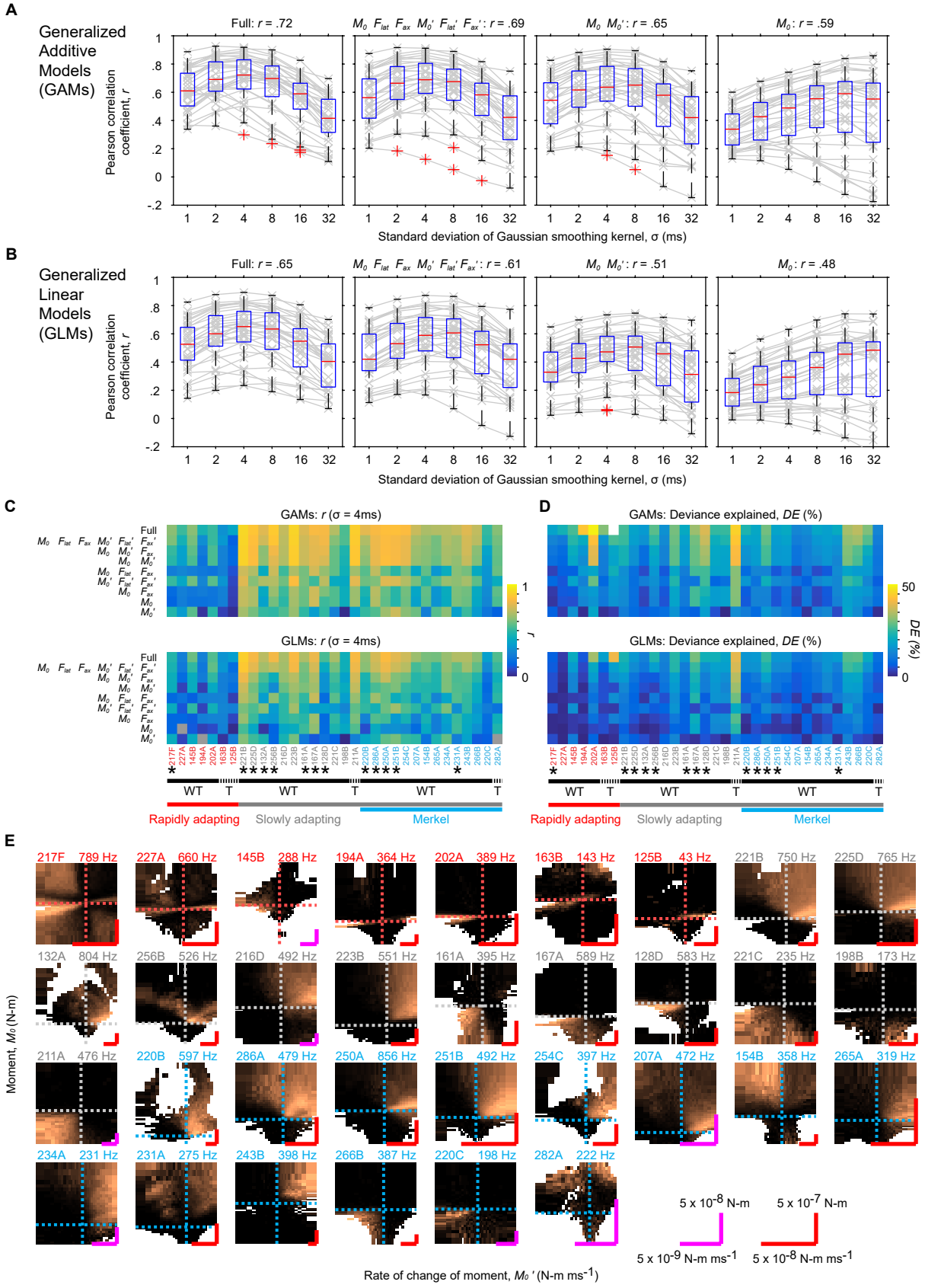
A
Generalized Additive Models (GAMs)
Full: r = .72
M0 Flat Fax M0' Flat' Fax': r = .69
M0 M0': r = .65
M0: r = .59
Pearson correlation coefficient, r
Standard deviation of Gaussian smoothing kernel, σ (ms)
B
Generalized Linear Models (GLMs)
Full: r = .65
M0 Flat Fax M0' Flat' Fax': r = .61
M0 M0': r = .51
M0: r = .48
Pearson correlation coefficient, r
Standard deviation of Gaussian smoothing kernel, σ (ms)
C
GAMs: r (σ = 4ms)
GLMs: r (σ = 4ms)
Full
r
WT T WT T WT T
Rapidly adapting
Slowly adapting
Merkel
D
GAMs: Deviance explained, DE (%)
GLMs: Deviance explained, DE (%)
DE (%)
WT T WT T WT T
Rapidly adapting
Slowly adapting
Merkel
E
217F 789 Hz
227A 660 Hz
145B 288 Hz
194A 364 Hz
202A 389 Hz
163B 143 Hz
125B 43 Hz
221B 750 Hz
225D 765 Hz
132A 804 Hz
256B 526 Hz
216D 492 Hz
223B 551 Hz
161A 395 Hz
167A 589 Hz
128D 583 Hz
221C 235 Hz
198B 173 Hz
211A 476 Hz
220B 597 Hz
286A 479 Hz
250A 856 Hz
251B 492 Hz
254C 397 Hz
207A 472 Hz
154B 358 Hz
265A 319 Hz
234A 231 Hz
231A 275 Hz
243B 398 Hz
266B 387 Hz
220C 198 Hz
282A 222 Hz
Moment, M0 (N-m)
5 x 10-8 N-m
5 x 10-7 N-m
5 x 10-9 N-m ms-1
5 x 10-8 N-m ms-1
Rate of change of moment, M0 ' (N-m ms-1)

Figure S2

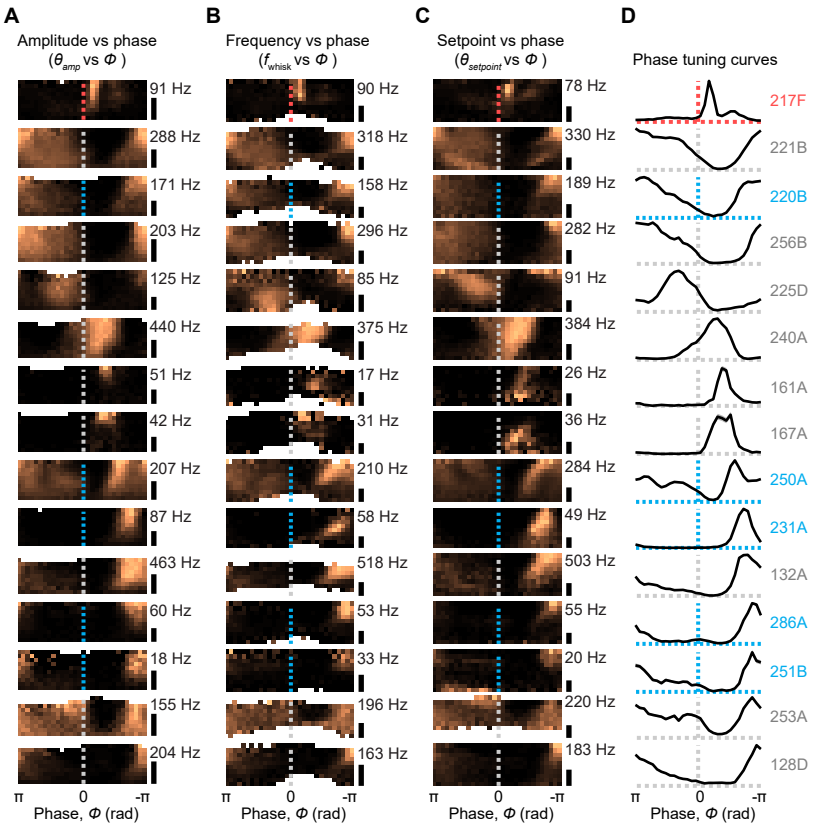
A
Amplitude vs phase
(θ_{amp} vs Φ)
91 Hz
288 Hz
171 Hz
203 Hz
125 Hz
440 Hz
51 Hz
42 Hz
207 Hz
87 Hz
463 Hz
60 Hz
18 Hz
155 Hz
204 Hz
π 0 -π
Phase, Φ (rad)
B
Frequency vs phase
(f_{whisk} vs Φ)
90 Hz
318 Hz
158 Hz
296 Hz
85 Hz
375 Hz
17 Hz
31 Hz
210 Hz
58 Hz
518 Hz
53 Hz
33 Hz
196 Hz
163 Hz
π 0 -π
Phase, Φ (rad)
C
Setpoint vs phase
($\theta_{setpoint}$ vs Φ)
78 Hz
330 Hz
189 Hz
282 Hz
91 Hz
384 Hz
26 Hz
36 Hz
284 Hz
49 Hz
503 Hz
55 Hz
20 Hz
220 Hz
183 Hz
π 0 -π
Phase, Φ (rad)
D
Phase tuning curves
217F
221B
220B
256B
225D
240A
161A
167A
250A
231A
132A
286A
251B
253A
128D
π 0 -π
Phase, Φ (rad)

Figure S3

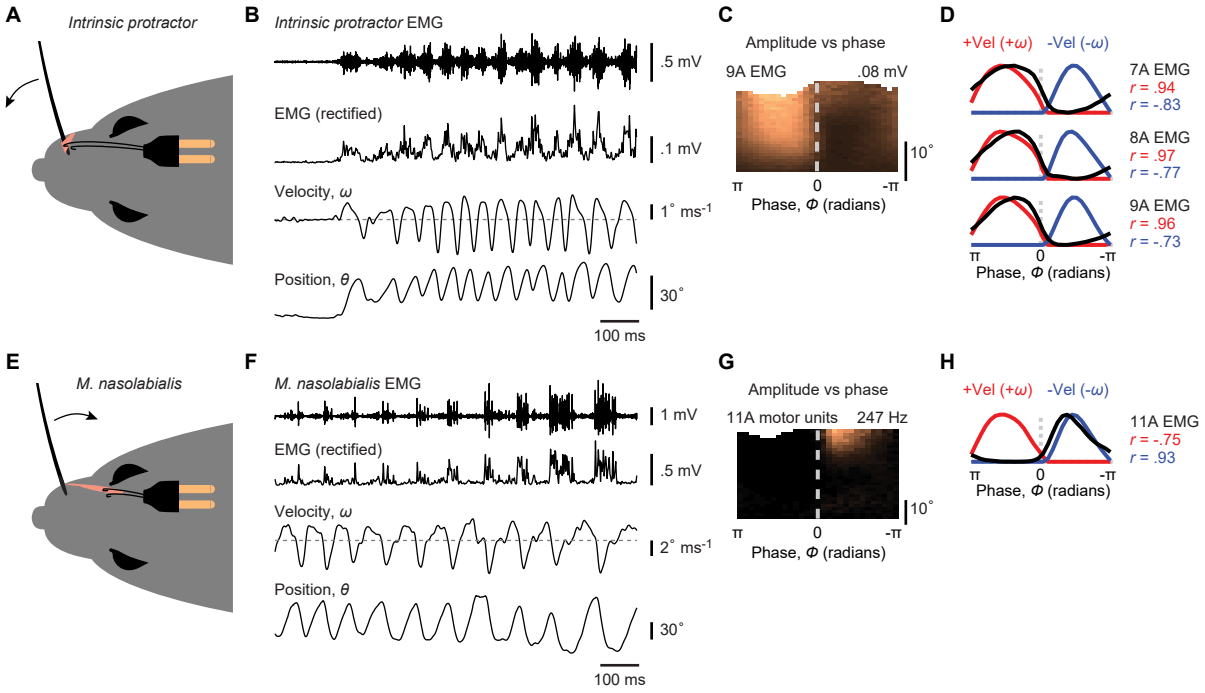
A
Intrinsic protractor
B
Intrinsic protractor EMG
.5 mV
EMG (rectified)
.1 mV
Velocity, ω
1˚ ms-1
Position, θ
30˚
100 ms
C
Amplitude vs phase
9A EMG
.08 mV
10˚
π
0
-π
Phase, Φ (radians)
D
+Vel (+ω)
-Vel (-ω)
7A EMG
r = .94
r = -.83
8A EMG
r = .97
r = -.77
9A EMG
r = .96
r = -.73
π
0
-π
Phase, Φ (radians)
E
M. nasolabialis
F
M. nasolabialis EMG
1 mV
EMG (rectified)
.5 mV
Velocity, ω
2˚ ms-1
Position, θ
30˚
100 ms
G
Amplitude vs phase
11A motor units
247 Hz
10˚
π
0
-π
Phase, Φ (radians)
H
+Vel (+ω)
-Vel (-ω)
11A EMG
r = -.75
r = .93
π
0
-π
Phase, Φ (radians)

Figure S4

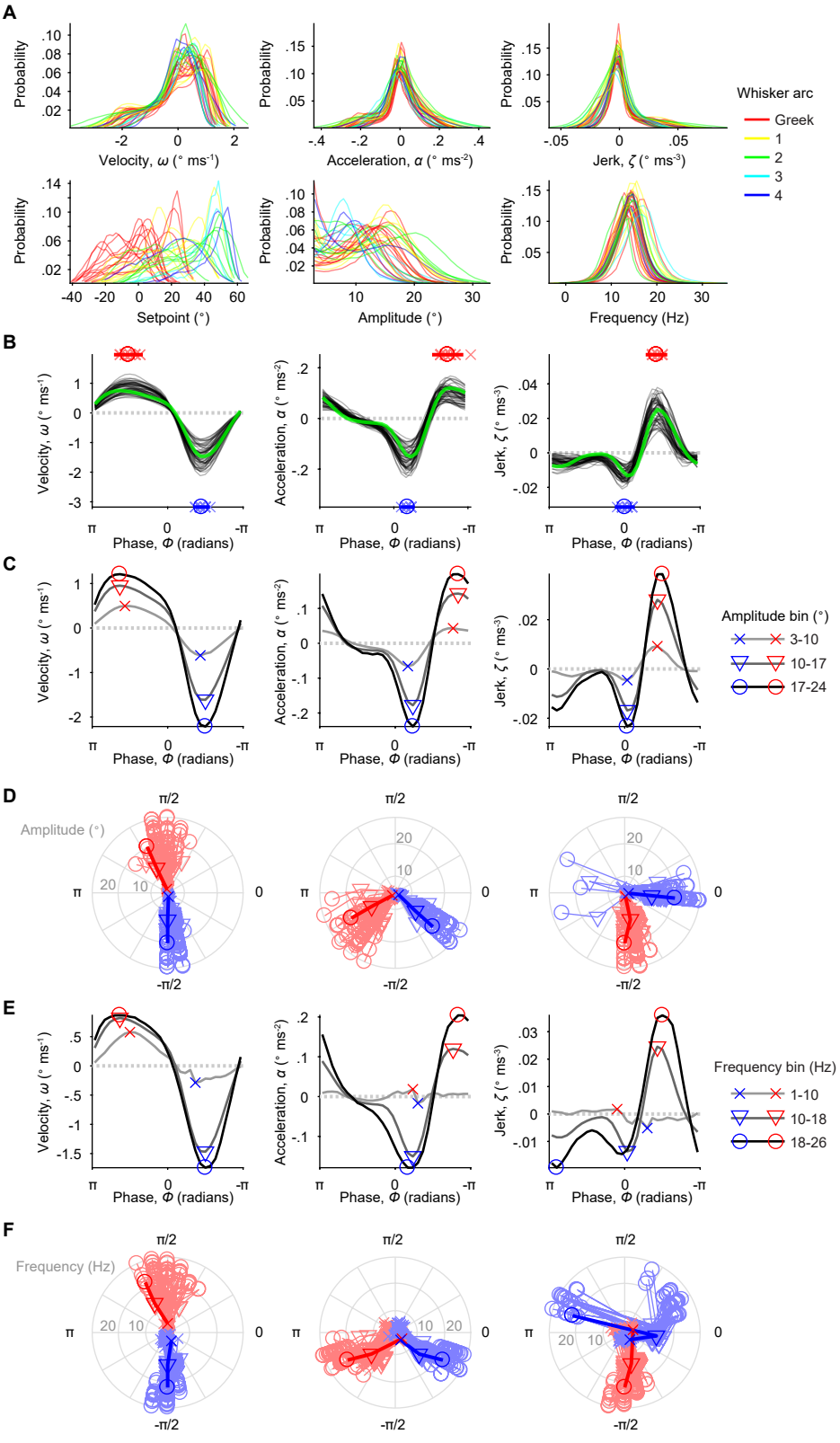
A
Probability
Velocity, ω (° ms-1)
Acceleration, α (° ms-2)
Jerk, ζ (° ms-3)
Setpoint (°)
Amplitude (°)
Frequency (Hz)
Whisker arc
Greek
1
2
3
4
B
Phase, Φ (radians)
C
Amplitude bin (°)
3-10
10-17
17-24
D
E
Frequency bin (Hz)
1-10
10-18
18-26
F

Figure S5

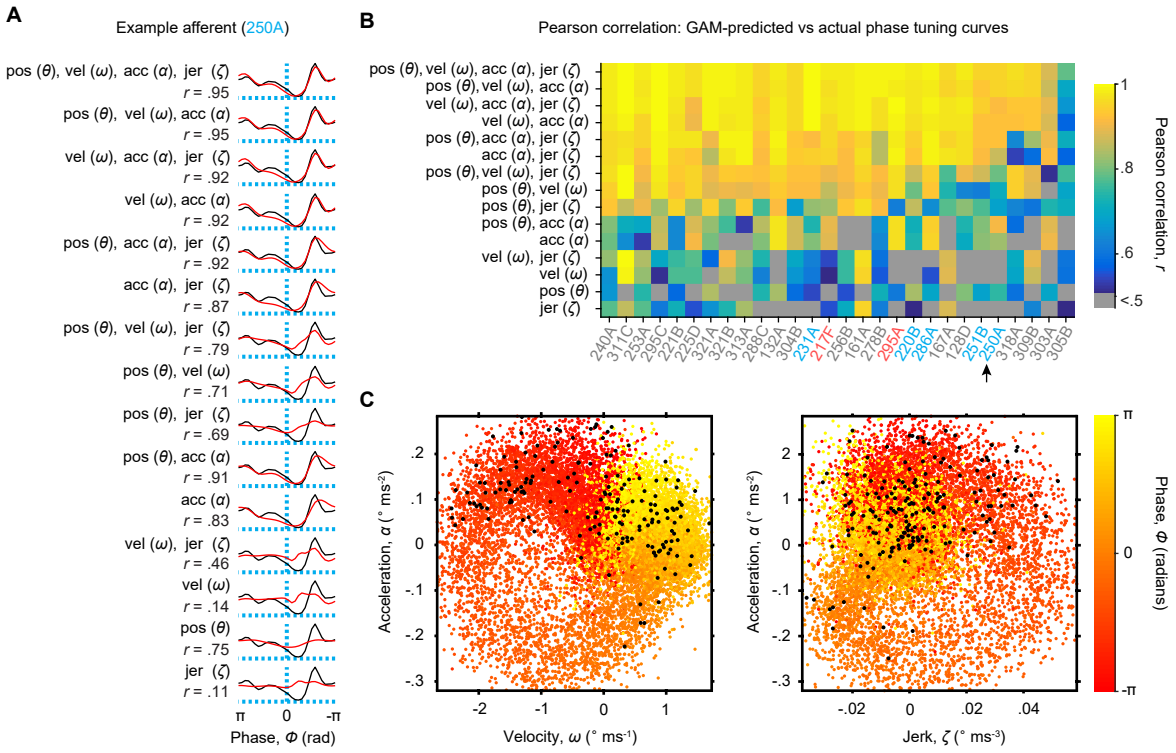
A
Example afferent (250A)
pos (θ), vel (ω), acc (α), jer (ζ) r = .95
pos (θ), vel (ω), acc (α) r = .95
vel (ω), acc (α), jer (ζ) r = .92
vel (ω), acc (α) r = .92
pos (θ), acc (α), jer (ζ) r = .92
acc (α), jer (ζ) r = .87
pos (θ), vel (ω), jer (ζ) r = .79
pos (θ), vel (ω) r = .71
pos (θ), jer (ζ) r = .69
pos (θ), acc (α) r = .91
acc (α) r = .83
vel (ω), jer (ζ) r = .46
vel (ω) r = .14
pos (θ) r = .75
jer (ζ) r = .11
π 0 -π
Phase, Φ (rad)
B
Pearson correlation: GAM-predicted vs actual phase tuning curves
pos (θ), vel (ω), acc (α), jer (ζ)
pos (θ), vel (ω), acc (α)
vel (ω), acc (α), jer (ζ)
vel (ω), acc (α)
pos (θ), acc (α), jer (ζ)
acc (α), jer (ζ)
pos (θ), vel (ω), jer (ζ)
pos (θ), vel (ω)
pos (θ), jer (ζ)
pos (θ), acc (α)
acc (α)
vel (ω), jer (ζ)
vel (ω)
pos (θ)
jer (ζ)
240A 311C 253A 295C 221B 225D 321A 321B 313A 288C 132A 304B 231A 217F 256B 161A 278B 295A 220B 286A 167A 128D 251B 250A 318A 309B 303A 303B
1 .8 .6 <.5
Pearson correlation, r
C
Acceleration, α (° ms-2)
.2 .1 0 -.1 -.2 -.3
-2 -1 0 1
Velocity, ω (° ms-1)
Acceleration, α (° ms-2)
2 1 0 -.1 -.2 -.3
-.02 0 .02 .04
Jerk, ζ (° ms-3)
π 0 -π
Phase, Φ (radians)

Figure S6

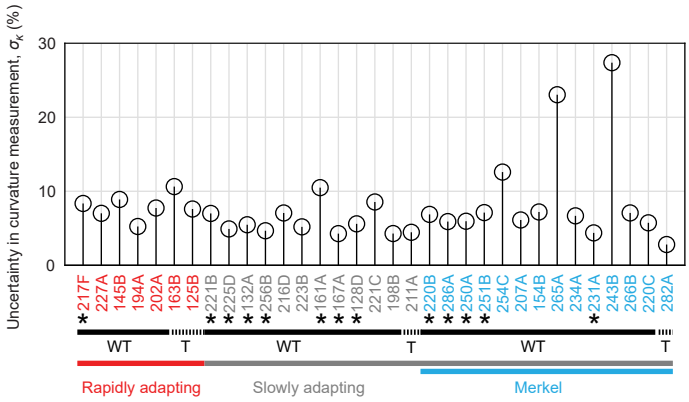
Uncertainty in curvature measurement, σ_κ (%)
30
20
10
0
217F
227A
145B
194A
202A
163B
125B
221B
225D
132A
256B
216D
223B
161A
167A
128D
221C
198B
211A
220B
286A
250A
251B
254C
207A
154B
265A
234A
231A
243B
266B
220C
282A
WT
T
WT
T
WT
T
Rapidly adapting
Slowly adapting
Merkel

Figure S7

Recording ID	Mouse ID	Sex	Mouse line	Recording Date	Type	Identified Merkel afferent	Receptive field	Whisker length (mm)	Whisker base radius (µm)	Whisking and touch sensitivity	Fitted by viscoelastic model	Appearances - Main Figures							Appearances - Supplemental Figures							Other notes
												Fig. 1	Fig. 2	Fig. 3	Fig. 4	Fig. 5	Fig. 6	Fig. 7	Fig. S1	Fig. S2	Fig. S3	Fig. S4	Fig. S5	Fig. S6	Fig. S7	
"Touch" recordings, with both whisker-pole contact and whisking in air																										
217F	KSt95	M	*TrKC^{CreER};Rosa^{Ai32}*	04/29/15	RA		ϖ	27.4	37.5	WT*	*N.A.*		C	C,D		C-E		B,G		A-E	A-D		A,B,D,F	B	A	
227A	KSt107	F	*TrKC^{CreER};Rosa^{Ai32}*	05/15/15	RA		ϖ	19.4	41.0	WT	*N.A.*		C	C,D				B		A-E			A,B,D,F		A	
145B	KSt76	M	*TrKC^{CreER};Rosa^{Ai32}*	09/27/14	RA		C3	11.7	30.5	WT	*N.A.*		C	C,D				B		A-E			A,B,D,F		A	
194A	KSt88	M	*TrKC^{CreER};Rosa^{Ai32}*	03/20/15	RA		ϖ	29.7	43.0	WT	*N.A.*		C	C,D				B		A-E			A,B,D,F		A	
202A	KSt92	M	*TrKC^{CreER};Rosa^{Ai32}*	04/05/15	RA		C2	17.2	38.5	WT	*N.A.*		C	C,D				B		A-E			A,B,D,F		A	
163B	KSt77	M	*TrKC^{CreER};Rosa^{Ai32}*	11/10/14	RA		ϖ	25.6	45.0	T	*N.A.*		C	C,D				B		A-E			A,B,D,F		A	
125B	KSt66	M	*TrKC^{CreER};Rosa^{Ai32}*	07/11/14	RA		C1	24.8	41.5	T	*N.A.*		C	C,D				B		A-E			A-F		A	
221B	KSt106	F	*TrKC^{CreER};Rosa^{Ai32}*	05/14/15	SA		β	28.3	44.5	WT*	Y		C	C,D	C	C-E		B,G		A-E	A-D		A,B,D,F	B	A	
225D	KSt107	F	*TrKC^{CreER};Rosa^{Ai32}*	05/14/15	SA		C2	16.4	39.0	WT*	Y	B	C	B,C,D,H	C	C-E		B,G		A-E	A-D		A,B,D,F	B	A	
132A	KSt69	M	*TrKC^{CreER};Rosa^{Ai32}*	07/25/14	SA		β	27.7	46.5	WT*	Y		C	C,D	C	C-E		B,G		A-E	A-D		A,B,D,F	B	A	
256B	KSt119	M	*TrKC^{CreER};Rosa^{Ai32}*	07/06/15	SA		C1	23.2	44.5	WT*	Y		C	C,D	C	C-E		B,G		A-E	A-D		A,B,D,F	B	A	
223B	KSt101	F	*TrKC^{CreER};Rosa^{Ai32}*	05/11/15	SA		ϖ	25.2	44.0	WT	Y		C	C,D	C			B		A-E			A,B,D,F		A	Example in Video S1
161A	KSt77	M	*TrKC^{CreER};Rosa^{Ai32}*	11/10/14	SA		D1	23.7	44.0	WT*	Y		C	C,D	C	C-E		B,G		A-E	A-D		A,B,D,F	B	A	
167A	KSt82	M	*TrKC^{CreER};Rosa^{Ai32}*	12/08/14	SA		C1	25.0	42.0	WT*	Y		C	C,D	C	C-E		B,G		A-E	A-D		A,B,D,F	B	A	
128D	KSt66	M	*TrKC^{CreER};Rosa^{Ai32}*	07/18/14	SA		ϖ	28.2	41.5	WT*	*N.A.*		C	C,D,I		C-E		B,G		A-E	A-D		A,B,D,F	B	A	
221C	KSt106	F	*TrKC^{CreER};Rosa^{Ai32}*	05/14/15	SA		β	28.3	44.5	WT	Y		C	C,D	C			B		A-E			A,B,D,F		A	
198B	KSt89	F	*TrKC^{CreER};Rosa^{Ai32}*	03/31/15	SA		ϖ	24.4	42.0	WT	Y		C	C,D	C			B		A-E			A,B,D,F		A	
216D	KSt97	M	*CCK^{Cre}; Rosa^{Ai32}*	04/27/15	SA		C3	11.1	28.0	T	Y		C	C,D	C			B		A-E			A,B,D,F		A	
211A	KSt96	F	*TrKC^{CreER};Rosa^{Ai32}*	04/20/15	SA		B2	14.1	28.5	T	Y		C	C,D,I	C			B		A-E			A,B,D,F		A	
220B	KSt99	M	*TrKC^{CreER};Rosa^{Ai32}*	05/06/15	SA	Y	C1	23.1	43.0	WT*	Y		B,C	C,D	C	C-E		B,G	C,D	A-E	A-D		A,B,D,F	B	A	
286A	KSt127	F	*TrKC^{CreER};Rosa^{Ai32}*	09/09/16	SA	Y	B2	15.0	37.0	WT*	Y		C	C,D	C	A-E		B,G	C,D	A-E	A-D		A,B,D,F	B	A	
250A	KSt115	F	*TrKC^{CreER};Rosa^{Ai32}*	06/22/15	SA	Y	β	20.1	41.0	WT*	Y		C	A,C-E,G,H	C	C-E		B,G	C,D	A-E	A-D		A,B,D,F	A-C	A	
251B	KSt117	M	*CCK^{Cre}; Rosa^{Ai32}*	06/29/15	SA	Y	B2	17.6	36.5	WT*	Y		C	C,D,H	B-D	C-E		B,G	C,D	A-E	A-D		A,B,D,F	B	A	
254C	KSt119	M	*TrKC^{CreER};Rosa^{Ai32}*	07/03/15	SA	Y	β	21.4	44.0	WT	Y		C	C,D	C			B	C,D	A-E			A,B,D,F		A	
207A	KSt91	M	*TrKC^{CreER};Rosa^{Ai32}*	04/13/15	SA	Y	C4	8.6	23.5	WT	Y		C	C,D	C			B	C,D	A-E			A,B,D,F		A	
154B	KSt80	F	*TrKC^{CreER};Rosa^{Ai32}*	10/25/14	SA	Y	δ	25.2	47.0	WT	Y		C	C,D	C			B	C,D	A-E			A,B,D,F		A	
265A	KSt122	M	*TrKC^{CreER};Rosa^{Ai32}*	07/19/15	SA	Y	D4	10.3	30.5	WT	Y		C	C,D	C			B	C,D	A-E			A,B,D,F		A	
234A	KSt111	M	*TrKC^{CreER};Rosa^{Ai32}*	05/29/15	SA	Y	C4	8.4	26.5	WT	Y		C	C,D	C			B	C,D	A-E			A,B,D,F		A	
231A	KSt109	F	*TrKC^{CreER};Rosa^{Ai32}*	05/21/15	SA	Y	C1	18.5	41.0	WT*	Y		C	C,D	C	C-E		B,G	C,D	A-E	A-D		A,B,D,F	B	A	
243B	KSt112	M	*TrKC^{CreER};Rosa^{Ai32}*	06/10/15	SA	Y	D2	20.1	38.0	WT	Y		C	C,D	C			B	C,D	A-E			A,B,D,F		A	
266B	KSt124	F	*TrKC^{CreER};Rosa^{Ai32}*	07/21/15	SA	Y	B1	24.2	44.5	WT	Y		C	C,D,I	C			B	C,D	A-E			A,B,D,F		A	
220C	KSt99	M	*TrKC^{CreER};Rosa^{Ai32}*	05/06/15	SA	Y	B3	11.3	27.0	WT	Y	D-F	C	C,D	C			B	C,D	A-E			A,B,D,F		A	
282A	KSt126	M	*TrKC^{CreER};Rosa^{Ai32}*	08/31/16	SA	Y	B3	8.1	22.5	T	Y		C	C,D	C			B	C,D	A-E			A,B,D,F		A	
"Touch" recordings excluded from all analysis except to quantify tagging method (Figure S1)																										
227C	KSt107	F	*TrKC^{CreER};Rosa^{Ai32}*	05/15/15	SA	Y	δ	26.3	41.0	WT	*N.A.*								C,D							Lack of rostral-caudal sensitivity prevented inclusion elsewhere
214A	KSt94	F	*TrKC^{CreER};Rosa^{Ai32}*	04/24/15	SA	Y	B1	20.1	39.0	WT	*N.A.*								C,D							Lack of rostral-caudal sensitivity prevented inclusion elsewhere
271A	KSt123	F	*TrKC^{CreER};Rosa^{Ai32}*	07/29/15	SA	Y	D1	22.8	40.0	*N.A.*	*N.A.*								C,D							Whisker tracking errors prevented inclusion elsewhere
"Cut whisker only" recordings obtained after the relevant whisker was cut (cf. Figure 7F)																										
199B	KSt89	F	*TrKC^{CreER};Rosa^{Ai32}*	04/01/15	SA	Y	D1 ✂	*N.A.*	*N.A.*	putative WT*	*N.A.*							B,F,G	C,D				A,B,D,F			
206A	KSt91	M	*TrKC^{CreER};Rosa^{Ai32}*	04/13/15	SA	Y	A1 ✂	*N.A.*	*N.A.*	putative WT*	*N.A.*							B,F,G	C,D				A,B,D,F			
209A	KSt93	M	*TrKC^{CreER};Rosa^{Ai32}*	04/16/15	SA	Y	A1 ✂	*N.A.*	*N.A.*	putative WT*	*N.A.*							B,F,G	C,D				A,B,D,F			
277A	KSm31	M	*Rosa^{Ai32}*	08/24/16	SA		E4 ✂	*N.A.*	*N.A.*	putative WT*	*N.A.*							B,F,G					A,B,D,F			
305A	KSt137	M	*Rosa^{Ai32}*	10/18/16	SA		α ✂	*N.A.*	*N.A.*	putative WT*	*N.A.*							B,F,G					A,B,D,F			
"Whisking in air without touch" recordings, whisker-pole contacts not analyzed due to too many whiskers in video																										
240A	KSt112	M	*TrKC^{CreER};Rosa^{Ai32}*	06/06/15	SA		B2	*N.A.*	*N.A.*	putative WT*	*N.A.*					C-E		B,G			A-D		A,B,D,F	B		
253A	KSt119	M	*TrKC^{CreER};Rosa^{Ai32}*	07/02/15	SA		C2	*N.A.*	*N.A.*	putative WT*	*N.A.*					C-E		B,G			A-D		A,B,D,F	B		
"Progressive whisker cutting" recordings, whisking in air without whisker-pole contact																										
278B	KSm30	M	*Rosa^{Ai32}*	08/31/16	SA		B2 → ✂	12.2	24.0	putative WT*	*N.A.*						E-G	B-E,G					A,B,D,F	B		
288C	KSt128	M	*TrKC^{CreER};Rosa^{Ai32}*	09/13/16	SA		B3 → ✂	10.7	27.0	putative WT*	*N.A.*						E-G	B-E,G					A,B,D,F	B		
295C	KSt131	M	*TrKC^{CreER};Rosa^{Ai32}*	09/23/16	SA		D1 → ✂	21.1	30.0	putative WT*	*N.A.*						B,E-G	B-E,G					A,B,D,F	B		Example in Video S2 - Episode 1
303A	KSt137	M	*Rosa^{Ai32}*	10/15/16	SA		D1 → ✂	24.4	43.5	putative WT*	*N.A.*						E-G	B-E,G					A,B,D,F	B		
304B	KSt137	M	*Rosa^{Ai32}*	10/17/16	SA		B2 → ✂	17.1	35.0	putative WT*	*N.A.*						E-G	B-E,G					A,B,D,F	B		
305B	KSt137	M	*Rosa^{Ai32}*	10/18/16	SA		B1 → ✂	24.7	44.5	putative WT*	*N.A.*						E-G	B-E,G					A,B,D,F	B		
309B	KSt135	M	*TrKC^{CreER};Rosa^{Ai32}*	10/24/16	SA		D2 → ✂	17.6	38.0	putative WT*	*N.A.*						D-G	B-E,G					A,B,D,F	B		
311C	KSt135	M	*TrKC^{CreER};Rosa^{Ai32}*	10/27/16	SA		C4 → ✂	9.8	24.5	putative WT*	*N.A.*						C,E-G	B-E,G					A,B,D,F	B		Example in Video S2 - Episode 2
313A	KSt138	M	*TrKC^{CreER};Rosa^{Ai32}*	11/20/16	SA		ϖ → ✂	21.5	46.5	putative WT*	*N.A.*						E-G	B-E,G					A,B,D,F	B		
318A	KSt140	M	*TrKC^{CreER};Rosa^{Ai32}*	12/01/16	SA		C1 → ✂	22.2	39.5	putative WT*	*N.A.*						E-G	B-E,G					A,B,D,F	B		
321A	KSt140	M	*TrKC^{CreER};Rosa^{Ai32}*	12/05/16	SA		D1 → ✂	22.3	45.0	putative WT*	*N.A.*						E-G	B-E,G					A,B,D,F	B		
321B	KSt140	M	*TrKC^{CreER};Rosa^{Ai32}*	12/05/16	SA		C3 → ✂	9.0	31.0	putative WT*	*N.A.*						E-G	B-E,G					A,B,D,F	B		
295A	KSt130	M	*TrKC^{CreER};Rosa^{Ai32}*	09/23/16	RA		D1 → ✂	18.6	28.5	putative WT*	*N.A.*						E-G	B-E,G					A,B,D,F	B		
EMG recordings, during whisking in air																										
7A	KSm6	M	*Rosa^{Ai32}*	06/02/16	*N.A.*	*N.A.*	*N.A.*	*N.A.*	*N.A.*	*N.A.*	*N.A.*							A,D,F,G				D				intrinsic protractor
8A	KSm8	M	*Rosa^{Ai32}*	06/04/16	*N.A.*	*N.A.*	*N.A.*	*N.A.*	*N.A.*	*N.A.*	*N.A.*							A,D,F,G				D				intrinsic protractor
9A	KSm9	M	*CCK^{CreER};Rosa^{Ai32}*	06/10/16	*N.A.*	*N.A.*	*N.A.*	*N.A.*	*N.A.*	*N.A.*	*N.A.*							A,D,F,G				B,C,D				intrinsic protractor
11A	KSm11	F	*Rosa^{Ai9}*	06/16/16	*N.A.*	*N.A.*	*N.A.*	*N.A.*	*N.A.*	*N.A.*	*N.A.*							A,D,F,G				F,G,H				extrinsic retractor

Table S1: Meta-data and assignment of neurons to analyses

Supplemental Figures

Figure S1. Specific labeling of Merkel afferents in TrkC^{CreER} mouse, related to Figure 1.

(A) Confocal stack projections of whisker follicles from two *TrkC^{CreER};Rosa^{Ai9}* mice (Mouse 1: top 4 rows; Mouse 2, bottom 4 rows). Green channel (left column, tdTomato) shows labeled afferent processes selected for classification of ending type (arrows). Endings that could not be identified by their morphology as a known whisker follicle ending type were "unclassified" (indicated by asterisks). In top left image, anatomical regions of the whisker are labeled: whisker shaft (arrowhead), ringwulst (RW), ring sinus (RS), and rete ridge collar (RRC). Merkel cells (middle column, magenta) were stained with anti-cytokeratin 8 (Krt8). Merged images (right column) were used to determine association of afferent endings with Merkel cells. All images are oriented with skin surface at the top. (B) Merkel cell-associated afferents are specifically labeled in whisker follicles of *TrkC^{CreER};Rosa^{Ai9}* mice (counts included all tdTomato^{+} afferents in 3 whisker pads from 3 mice). Of classified Merkel afferents, the vast majority (994 of 1,045) were located in the Merkel dense region rather than the rete ridge collar. (C) Mean spike waveforms evoked by light (blue: *TrKC^{CreER};Rosa^{Ai32}* mice; green: *Cck^{Cre};Rosa^{Ai32}*) shown superimposed on those evoked by mechanical stimulation (black). Spike latency is indicated above each waveform (mean ± SD from time of light onset to spike peak or trough, in ms). All identified Merkel afferents are shown (n = 19 from *TrKC^{CreER};Rosa^{Ai32}* in blue, and n = 1 from *Cck^{Cre};Rosa^{Ai32}*in green; Table S1). Three putative WT* afferents from Figure 7F, obtained after whisker cutting, are indicated with scissors icons. To help characterize our optogenetic tagging method, also shown are 3 afferents (bottom row, right-most) for which lack of rostral-caudal direction selectivity or whisker tracking errors prevented inclusion in other figures or analyses (Table S1). Spike waveforms presumably vary in part to electrode position with respect to the cell body and axon of these pseudounipolar neurons. (D) Histogram of mean spike latencies for the neurons in (C).

Figure S2. Tuning to contact forces and bending moment, related to Figure 3 and Figure 4.

(A) Systematic evaluation of the performance of Generalized Additive Models (GAMs) fitted by different combinations of variables (shown in title of each plot) during contact periods for each neuron (gray lines; n = 33 afferents in each plot). The *r* value given in the title is the median Pearson correlation coefficient across neurons for the level of smoothing yielding highest performance. "Full" models include all dynamic variables (M_0, F_{ax}, F_{lat}) and their rates of change (M_0', F_{ax}', F_{lat}'), plus four kinematic variables (θ, ω, α, ζ). The performance of each model (gray crosses) was quantified as the Pearson correlation coefficient (*r*; y-axis) between predicted spike rate and the recorded spikes smoothed by Gaussian kernels with a range of sizes (in standard deviation, σ; x-axis). Box plots depict distribution of *r* values across neurons within each smoothing condition (medians: red lines; 25th and 75th percentiles: lower and upper box boundaries; outliers marked by red plus symbols; MATLAB "boxplot"). Most models achieved best performance with σ = 4 ms. (B) Evaluation of Generalized Linear Models (GLMs) for the same data showing similar relationships between model performance and the smoothing parameter. Conventions as in (A). (C) Heatmaps showing *r* values (σ = 4 ms) for GAMs (top) and GLMs (bottom) based on different combinations of mechanical variables (along rows) for each neuron (columns). Similar to Figure 3D but including additional models. Afferents are sorted and labeled along the x-axis identically to Figure 2C, and are also listed by name to allow identification in Table S1. Conventions as in Figure 2C. GAMs outperform GLMs overall. (D) Same as in (C) but with performance quantified using deviance explained (%), which does not depend on smoothing. (E) Tuning surfaces for moment and its rate of change, for all touch recordings (n = 33). Dashed lines indicate the origin of each axis and are colored by afferent type (blue: Merkel; gray: SA; red: RA). The color scale for each surface ranges from 0 Hz to a maximum spike rate indicated by text above the surface (in Hz). Viscoelastic model was fitted to all Merkel and SA afferents except for 128D (for which the fitting algorithm failed). Red scale bars indicate 5 x 10^{-7} N-m and 5 x 10^{-8} N-m ms^{-1} for M_0 and M_0', respectively. Magenta scale bars indicate 5 x 10^{-8} N-m and 5 x 10^{-9} N-m ms^{-1} for M_0 and M_0', respectively. Bins with fewer than 25 observations are white.

Figure S3. Phase tuning during whisking in air across amplitudes, frequencies and setpoints, related to Figure 5.

(A) Tuning surfaces for each afferent (n = 15 WT* afferents, arrayed vertically), showing spike rate binned by both phase (x-axis) and whisk amplitude (y-axis; scale bars: 10°). Color scale for each surface spans 0 Hz to a maximum firing rate (in Hz) indicated to the right of each panel. Vertical dashed lines mark phase of 0 and are colored according to afferent type (blue: Merkel; gray: SA; red: RA). (B) Tuning surfaces for the same neurons (rows aligned with A) but with spike rate binned by phase (x-axis) and frequency (y-axis; scale bars: 10 Hz). (C) Tuning surfaces for the

same neurons (rows aligned with A), but with spike rate binned by phase (x-axis) and setpoint (y-axis; scale bars: 20°). (D) Phase tuning curves normalized and in Cartesian coordinates (mean ± SEM spike rate) for each neuron (rows aligned with A). Axes are colored by afferent type as in (A). Unit names are listed to allow identification in Table S1.

Figure S4. Electromyogram (EMG) recordings from muscles that drive whisking, related to Figure 7.

(A) Schematic of chronic EMG recording procedure targeting intrinsic protractor muscle. During implantation of electrodes at this site, current stimulation resulted in whisker protraction. (B) Example EMG signal recorded together with high-speed whisker video during exploratory whisking. Rectified EMG signals were averaged into 2 ms bins. Intrinsic protractor activity peaked while velocity (ω) was positive, prior to peak position (θ). (C) Tuning surface for intrinsic protractor recording in (B), showing mean rectified EMG as a function of whisk phase (x-axis) and amplitude (y-axis, scale bar: 10°) measured from high-speed video (30 equally spaced bins for both phase and amplitude). Color ranges from 0 (black) to 0.08 mV. (D) Traces of mean rectified EMG (black curves) as a function of phase, for each of three intrinsic protractor recordings. Traces of mean whisker velocity as a function of phase were split into positive (red) and negative (blue) values, rectified and overlaid for each recording. Pearson correlation coefficients shown at right indicate that intrinsic protractor muscles and positive velocity were highly correlated within whisk cycles. (E) Schematic of chronic EMG recording procedure to target the extrinsic retractor muscle *m. nasolabialis*. During electrode implantation, passing current resulted in whisker pad retraction. (F) Example EMG signal for *m. nasolabialis*, with whisker velocity and position from high-speed video. Motor unit spikes were prevalent in this recording. Extrinsic retractor activity peaked while velocity was negative, just after peak position. (G) Same as (C), but based on motor unit spike rate. Color ranging from 0 (black) to 247 Hz. (H) Same as D, but for *m. nasolabialis* recording, showing high correlation with negative velocity within whisk cycles.

Figure S5. Distributions of kinematics and degree of invariance of kinematics with phase, related to Figure 7.

(A) Traces in each panel show probability distributions of a kinematic variable (indicated under each plot) for individual recording sessions (n = 33 sessions). Colors indicate whisker arc (columnar identity in whisker array on face). (B) Traces show the mean velocity (left), acceleration (middle), or jerk (right) binned by phase (x-axis) for the recording sessions in (A). Green traces show one example session. Crosses indicate the phases at which positive (red) and negative (blue) peaks occur for individual traces. Corresponding circles and error bars show the mean ± 3 SD of these peaks. (C) Mean kinematics binned by phase (x-axis) and amplitude (grayscale traces; bins indicated in legend at right) for the example session (green curves) in (B). Markers indicate the phases where positive (red) and negative (blue) peaks occur for low (cross), middle (triangle), and high (circle) amplitude bins, respectively. (D) For all sessions, phase (angular axis) and amplitude (radial axis) values of the peaks extracted as in (C). Color and symbol conventions as in (C). Peaks from the same sessions are connected by lines. Data from the example session in (B) are plotted with thick lines. (E, F) Similar to (C, D) but for whisk frequency instead of whisk amplitude. The phases where peaks in kinematics occur are largely invariant across amplitudes and frequencies, except for negative jerk.

Figure S6. Phase tuning in terms of instantaneous combinations of kinematic variables, related to Figure 7.

(A) Each row shows an overlay of the observed phase tuning curve (black, same in each row) for an example Merkel afferent and a tuning curve predicted from a GAM model (red) fitted to one of 15 possible combinations (indicated at left) of four kinematic variables (θ, whisker position; ω, velocity; α, acceleration; ζ, jerk) during whisking in air. Pearson correlation coefficient between observed and predicted curves, r, is shown to the right for each row. (B) Heatmap of r quantified as in (A) for each model type (kinematic variables listed at left) for all WT* neurons (columns). Gray indicates r values < 0.5. Arrow indicates the example afferent from (A). Afferent names along the x-axis are colored by afferent type (blue: Merkel; gray: SA; red: RA). Models containing at least acceleration and velocity (or jerk) produced good performance, while those lacking acceleration generally performed worse. (C) Spikes during whisking in air are triggered in a confined region of kinematic subspace, giving rise to phase tuning (inspired by Wallach et al. 2016). Left, Each point in the background is the instantaneous acceleration (y-axis), velocity (x-axis), and phase (color) for a random subset of frames (15,000 out of ~590,900 total) for the example afferent in (A). In the foreground, another random subset of frames were drawn (1,500 of ~590,900) and those with spikes were plotted as black dots. Right, Same as left panel but acceleration and jerk, and with different randomly chosen frames.

Figure S7. Uncertainty level of curvature change measurements, related to Figure 3.

The uncertainty or "noise" level (σ_κ) for the curvature measurement in each touch recording (n = 33) is the ratio of mean curvature change measured in the absence of contact to that measured in the presence of contact (STAR Methods). Afferents are sorted and labeled along the x-axis identically to Figure 2C, and are also listed by name to allow identification in Table S1. Conventions as in Figure 2C.

Table S1. Meta-data for all recordings and their assignment to analyses, related to STAR Methods.

Metadata for each afferent, including figure appearances. Scissors icons indicate a receptive field comprising a whisker cut to within ~1.2 mm or less from the face. T: sensitive to touch, but not to whisking. WT: sensitive to both whisking and touch. WT*: sensitive to both whisking and touch, with mean whisking in air spike rate >1 Hz and >1000 spikes. *N.A.*: not applicable.